Polymer Chemistry

PAPER

View Article Online
View Journal | View Issue

Cite this: *Polym. Chem.*, 2014, **5**, 6216

Monosaccharide-functionalized poly(phenylacetylenes): *in situ* polymerization, hybridization with MWCNTs, and application in the reinforcement of chitosan rods†

Xiao Wang,[a] Yuan Gao,[a] Hui Zhao,‡[a] Xiao-Qing Liu,§[a] Zhengke Wang,[a] Anjun Qin,[a,b] Qiaoling Hu,[a] Jing Zhi Sun*[a] and Ben Zhong Tang*[a,b,c]

Received 10th June 2014,
Accepted 4th July 2014

DOI: 10.1039/c4py00809j

www.rsc.org/polymers

Monosaccharide-functionalized poly(phenylacetylenes) (PPAs) are synthesized with high yield and molecular weight, but it shows no solvating power to multiwalled carbon nanotubes (MWCNTs) by simply blending them together. Polymerization of monosaccharide-functionalized monomers in the presence of MWCNTs (*in situ* polymerization) leads to the hybrids of monosaccharide-functionalized PPAs/MWCNTs, and the content of MWCNTs is over 2% by weight. The characterization data indicates that the π–π interaction between the styrene-like moieties in the polymer backbone and the MWCNTs plays crucial role in the dispersing capacity. Based on the *in situ* precipitation method, CS rods containing monosaccharide-functionalized PPAs/MWCNTs hybrids were fabricated. The bending strength and modulus of the hybrid-reinforced CS rods showed substantial improvement in comparison with the CS rods made from pristine and hydroxyapatite-reinforced CS.

Introduction

Polyacetylene derivatives have been furnished with a variety of functions, including photo-conductivity, gas permeability, liquid crystal property, polymer main chain chirality, and inorganic-hybridization ability by the polymerization of the intentionally designed monomers.[1–10] Among the versatile potentialities in practical application, the biologically inspired functional polyacetylenes is one of the most attractive research topics, although the reports are relatively lacking in comparison with other kinds of functional polyacetylenes.[11–15] The first bioinspired species was a polyacetylene derivative bearing L-valine pendants, which was reported in 2001.[11,12] The polymers modified by amino acids showed good cytocompatibility.[13] When living cells were subcultured in the microtiter plates precoated with the polymer film, the cells adhered to and grew well on the plates, similar to the behavior observed for the control samples. Polyacetylenes bearing monosaccharide pendants played a role of nutrition, and the prolification rate was doubled when the cells were cultured in the media containing proper amount of monosaccharide-modified polyacetylenes.[14,15] These results suggested that bio-molecularly functionalized polyacetylenes can be promising candidates for the fabrication of tissue-engineering materials.

A recent progress was addressed by Wang and colleagues.[16] In this work, the substantial reinforcement of chitosan (CS) rods was achieved by introducing nanohybrids composed of components of an amino-functionalized poly(phenylacetylene) (PPA) and multi-walled carbon nanotubes (MWCNTs). CS has been proved to be biocompatible, biodegradable, and capable of inherent wound healing.[17–20] However, the pristine CS is unprocessable because of the strong multiple intermolecular

[a]*MOE Key Laboratory of Macromolecular Synthesis and Functionalization, Department of Polymer Science and Engineering, Zhejiang University, Hangzhou 310027, China. E-mail: sunjz@zju.edu.cn; Fax: +86-571-87953734; Tel: +86-571-87953734*

[b]*Guangdong Innovative Research Team, State Key Laboratory of Luminescent Materials and Devices, South China University of Technology, Guangzhou 510640, China*

[c]*Department of Chemistry, Jockey Club Institute for Advanced Study, Institute of Molecular Functional Materials, State Key Laboratory of Molecular Neuroscience, and Division of Biomedical Engineering, The Hong Kong University of Science & Technology, Clear Water Bay, Kowloon, Hong Kong, China. E-mail: tangbenz@ust.hk; Fax: +86-852-2358-7375; Tel: +86-852-2358-1594*

†Electronic supplementary information (ESI) available: Synthetic details for the monomers; FTIR and ^{1}H NMR spectra of **1** and **P1**, ^{13}C NMR spectra of **1** and **P1**; CD spectra of **M1** at different temperatures, thermograms for **P1** and **P1**@MWCNTs. See DOI: 10.1039/c4py00809j

‡Present address: Weizmann Institute of Science, Israel. Fax: +972-8-934-4107.

§Present address: College of Chemistry and Molecular Engineering, Peking University, Beijing 100871, China. Tel:/Fax: +86-10-62753370.

hydrogen bonding. Since the discovery of the *in situ* precipitation strategy,[21,22] CS-based devices can be fabricated into various shapes and dimensions.[22–25] Thus, CS becomes a kind of promising material to be used as temporary mechanical supporting components for the regeneration of bone. The bending strength and bending modulus of the CS rods made from *in situ* precipitation are 92.4 MPa and 4.1 GPa, respectively. As for CS/hydroxyapatite composite rods, these two indexes dropped to 86.0 MPa and 3.4 GPa, respectively.[22] Rigid and brittle inorganic fillers can help greatly to enhance the strength and decrease strain, but they are helpless to improve their bending strength. Practically, the bending strength and bending modulus of the commercial nails produced by Dikfix are 130 MPa and 2.0–3.0 GPa, respectively.[22] The bending strength and bending modulus of the CS rods containing hybrid of amino-functionalized PPA/MWCNTs are as high as 124.6 MPa and 5.3 GPa, corresponding to the enhancement of 34.8% and 29.3%, in comparison with the pristine CS rods.[16] The amino-functionalized PPA or poly(*p*-amino-phenylacetylene) played a key role in the incorporation of MWCNTs into CS rods. The non-processable MWCNTs became processable due to the wrapping of the polymer chains on the surface of MWCNTs through the π–π interactions between the poly(phenylacetylene) backbone and MWCNTs. Poly(*p*-aminophenylacetylene) could be dissolved in acidic aqueous solutions due to the protonation of the aniline moieties, thereby the surface-decorated MWCNTs could be introduced into the acidic aqueous solution of CS matrix. In this work, the advantage of the conjugated π-electronic structure of poly(phenylacetylene) was taken into account to improve the performance of biomaterials.

The MWCNTs content in the obtained CS matrix was only about 1.34% by weight, because the solubility of poly(*p*-aminophenylacetylene) in aqueous media was limited.[16] To make full use of the mechanical strength of such small amount of MWCNTs, magnetic Fe_3O_4 particles were simultaneously deposited onto MWCNTs to help the MWCNTs align in the axial direction of CS rods during the molding process. In addition to the limited amount of MWCNTs, some undesirable effects emerged because of the presence of Fe_3O_4 component. For example, the CS rods are of ferruginous color, which is unpleasant looking. Despite the experimental evidence of being non-harmful to cells and tissues, the long-term stability and biocompatibility of the aniline-like moieties in poly(*p*-aminophenylacetylene) need to be evaluated.

In these points of view, it is of great significance to develop other biocompatible polyacetylenes that can help to disperse MWCNTs into the CS matrix without the unwanted effects. To this end, we planned to replace the poly(*p*-amino-phenylacetylene) component by monosaccharide-functionalized poly(phenyl-acetylenes) in order to make use of their good water solubility and cytocompatibility. Based on our previous works,[12–15] the monosaccharide moieties bestow the polymers with good solubility in aqueous media, and the PPA backbone endows the polymers with the possibility to wrap onto MWCNTs' surface *via* π–π interaction. Herein, we report the preparation of these monosaccharide-functionalized poly(phenylacetylenes), the interaction between the polymer chains and MWCNTs, and the mechanical properties of CS rods reinforced by MWCNTs decorated with monosaccharide-functionalized poly(phenylacetylenes).

Results and discussion

Preparation of the monosaccharide-functionalized phenylacetylene monomers and polymers

The synthetic route to the monosaccharide-functionalized phenylacetylenes (**1**, **2** and **3**) is shown in Scheme 1. The experimental details and characterization data are included in the Experimental section and can also be found in literature.[14] In the pristine monosaccharides (D-glucose, D-mannose and D-galactose), there are five hydroxyl groups, which should be selectively protected to avoid the side reactions with 4-ethynylbenzoic acid (**7**) and their poisoning effects on the successive polymerization catalyst. The synthetic route is displayed in Scheme S1.† The monomers **1**, **2** and **3** were prepared by the esterification reaction of **7** with acetone protected monosaccharides (**8**, **9** and **10**), which was obtained by the condensation between the 1,2-diol groups of the monosaccharide and acetone in the presence of H_2SO_4 and $CuSO_4$.

The monomers were polymerized under the catalyzing action of organorhodium complexes $[Rh(diene)Cl]_2$, which are widely used in the polymerization of phenylacetylene derivatives.[3,9,10] We attempted the polymerization by using two kinds of $[Rh(diene)Cl]_2$ (*i.e.*, $[Rh(nbd)Cl]_2$ and $[Rh(cod)Cl]_2$) in THF solvent and in the presence of trace amount of dried Et_3N. The polymerization went on efficiently and the target polymers were produced in high yield and high molecular weight. The data are summarized in Table 1. For example, the yield of D-mannose-functionalized PPA was 95% and 87% under the catalyzing of $[Rh(nbd)Cl]_2$ and $[Rh(cod)Cl]_2$, and the corresponding molecular weight was (M_w) 169 400 and 157 100 (Table 1, no. 1 and 2), respectively. The chemical structures of the derived polymers were characterized with multiple spectro-

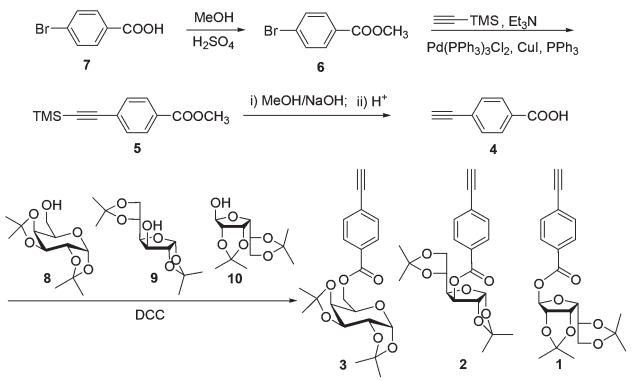

Scheme 1 Synthetic route to the functionalized poly(phenylacetylenes) with a protected monosaccharide pendent.

Table 1 Polymerizations of functionalized phenylacetylene monomers bearing protected monosaccharides[a]

No.	M[b]	Catalyst	Colour	Yield (%)	M_w [c]	M_w/M_n [c]
1	**1**	$[Rh(nbd)Cl]_2$	Brown	95	169 400	1.93
2	**1**	$[Rh(cod)Cl]_2$	Brown	87	157 100	2.13
3	**2**	$[Rh(nbd)Cl]_2$	Red	87	176 400	1.49
4	**2**	$[Rh(cod)Cl]_2$	Red	82	168 600	2.02
5	**3**	$[Rh(nbd)Cl]_2$	Brown	98	72 400	2.81
6	**3**	$[Rh(cod)Cl]_2$	Brown	87	355 900	4.98

[a] Carried out at room temperature under nitrogen for 24 h, $[M]_0$ = 0.125 M. [cat.] = 1/20 $[M]_0$. [b] M = monomer. [c] Determined by GPC in THF on the basis of a polystyrene calibration.

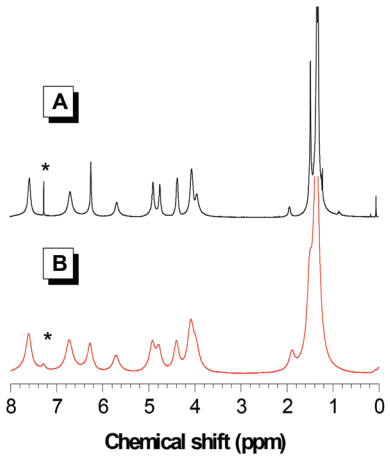

Fig. 1 ^1H NMR spectra of D-mannose-functionalized poly(phenylacetylene) (P**1**) obtained by polymerization of **1** in THF solution (A) and *in situ* polymerization **1** in the presence of MWCNTs (B). Solvent: $CDCl_3$, the solvent peaks are marked as asterisks.

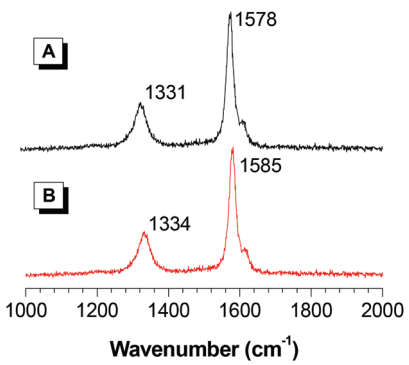

Fig. 2 Raman spectra of MWCNTs (A) and P**1**/MWCNTs (B).

scopic techniques and the results are described in the Experimental section and discussed below (*cf.* Fig. 1–3).

Preparation of hybrids of polymer/MWCNTs

With these products (P**1**, P**2** and P**3**), we attempted to prepare the hybrids of functionalized PPAs and MWCNTs. In our previous works, the hybrids of functionalized PPAs and MWCNTs or single-walled carbon nanotubes were derived readily by

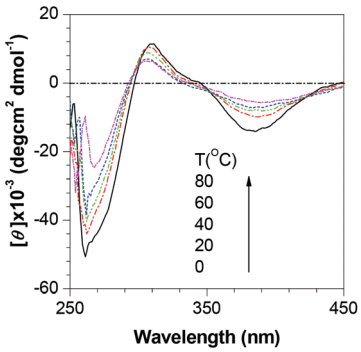

Fig. 3 The circular dichroism spectra of P**1**/MWCNTs at temperature of 0, 20, 40, 60, 80 °C. Polymer concentration: 0.1 mM; Solvent: DMF.

simply blending the two components together in a suitable solvent.[2,26–30] Similarly, we mixed P**1** with proper amount of pretreated MWCNTs in THF solvent under stirring. Unfortunately, this process did not work for P**1**. After filtering and washing with THF, the filtrate was a clear light yellow solution, while all of the added WMCNTs were collected in the cotton filter. This observation indicates that the interactions between P**1** and MWCNTs are too weak to help the dispersion of MWCNTs in solvents. Moreover, we attempted the hybridization of P**2** and P**3** with MWCNTs by solution blending technique, but both failed to provide the expected hybrids. Upon analyzing the solvating power of PPA derivatives to MWCNTs, we realized that polymer chains of the monosaccharide-functionalized PPAs cannot wrap onto the surface of MWCNTs, because on one hand, the monosaccharide groups are hydrophilic but the surface of MWCNTs is hydrophobic, whereas on the other hand, the pendent monosaccharide-moieties around the polymer main chain hinder the π–π interaction between PPA chains and MWCNTs.

To take advantage of the π–π interaction between PPA and MWCNTs, we tried the *in situ* polymerization of monosaccharide-functionalized monomers using $[Rh(nbd)Cl]_2$ as catalyst. The reaction conditions were similar to that described above, and the only difference is the presence of MWCNTs in the polymerization process. As expected, yellowish-black suspensions were formed after reacting for 24 h. After removing the insoluble MWCNTs by filtration, dark yellowish-green filtrate was obtained. The color change indicated the dispersion of MWCNTs in the solution. After drying, the resultant powder took a greyish-green color, indicating the coexistence of polymers and MWCNTs. By repeated washing with THF, the polymers and MWCNTs could be separated and the obtained pure polymers were sent for molecular weigh estimation and structural characterization. The characterization data are summarized in Table 2 and Fig. 1–3. It was found that the products had similar molecular weights and polydispersity indexes (PDI) to that obtained by solution polymerization (comparing the data in Tables 1 and 2); however, the overall yield became lower (for **M1**, 80% *versus* 87%). The decrease is caused by the weight loss from the repeated washing procedure. In addition to the good yield and high molecular weight, the obtained

Table 2 *In situ* polymerizations of monosaccharide-functionalized phenylacetylene monomers in the presence of MWCNTs[a]

No.	M[b]	Colour	Yield (%)	M_w [c]	M_w/M_n [c]	C[d] (%)
1	**1**	Dark green	80	165 200	1.95	2.10
2	**2**	Dark green	61	256 300	1.97	2.35
3	**3**	Dark green	87	237 200	2.54	2.79

[a] Carried out at room temperature under nitrogen for 24 h, $[M]_0$ = 0.125 M. [cat.] = 1/20 $[M]_0$. [b] M = monomer. [c] Determined by GPC in THF on the basis of a polystyrene calibration. [d] *C* = content of MWCNTs by weight.

hybrids were easy to be re-dispersed in common organic solvents, such as THF, DMF, chloroform and dichloromethane, to give rise to a light yellow solution. The content of MWCNTs in the hybrid derived from *in situ* polymerization is over 2.0% (Table 2, by weight). The calculation is based on the method reported in previous works.[26]

The structure of the polymers obtained by intrinsic solution polymerization *in situ* polymerization was characterized by using spectroscopic methods, including FTIR, ^{1}H NMR and ^{13}C NMR (Fig. 1, S1–S3†). The analyzed data were in good agreement with the expected molecular structures (see Experimental section for the detailed assignment). Herein, we use **P1** and **M1** as representatives to show that the *in situ* polymerization scheme has little effects on the polymer structure. The FTIR spectra of **P1** and **1** are shown in Fig. S1.† For **1**, the spectrum displays the absorption bands at 3272 and 2110 cm^{-1}, which are ascribed to the stretching vibrations of ≡C–H and C≡C, respectively. Both of them are absent in the spectrum of **P1**, indicating that the triple bond of **1** has been completely consumed during the polymerization process. Moreover, a strong band at around 1730 cm^{-1}, which is assigned to stretching vibration of C=O group, is retained in the spectra of both **1** and **P1**, indicating that the ester linkage is intact between the phenyl and monosaccharide during the polymerization.

Further proof for confirming the polymerization are revealed by both ^{1}H NMR and ^{13}C NMR measurements (Fig. 1, S2 and S3†). The ^{1}H NMR spectra of **P1** and **1** are shown in Fig. 1. For **1**, the peak around $\delta \sim 3.26$ is assigned to the acetylene proton, whereas in the spectrum of **P1**, this peak disappears while a new peak associated with the resonance of olefinic protons appears at $\delta \sim 5.67$, indicating that the acetylenic triple bond in **1** has been transformed to the olefinic double bond in **P1** by the polymerization reaction. The appearance of the olefinic protons at $\delta \sim 5.67$ suggests that the polymer backbone has a *cis*-rich configuration.[31] The *cis*-content can be estimated by ^{1}H NMR spectroscopic method, in which the chemical shift of $\delta \sim 5.7$ ppm is assigned to the *cis*-proton. Based on our previous work, we estimated the *cis*-contents of **P1** in its pristine and hybrid forms are 93.6% and 85.5%, respectively. The data indicates that the presence of MWCNTs really has effect on the *cis*-content of the resultant polymers. In addition, the up-field shifted resonance of the phenyl protons from $\delta \sim 7.41$ and 6.82 to $\delta \sim 6.62$ and 6.44 further indicate the formation of polyene backbone (peaks b and c in Fig. S2†), because the conjugation between the polyene main chain and phenyls should induce an up-field shift of the protons' resonance.

The ^{1}H NMR spectrum of the *in situ* polymerization resultant disclose information about hybridization. Comparing the chemical shifts of the related protons for **P1** and its hybrid with MWCNTs (Fig. 1A and 1B), it is found that the δ values have little changes, but the peaks become broader. Based on the principle of NMR spectroscopy, peak-broadening indicates the restriction of the free rotations of the groups onto which the protons are attaching, because the restriction can make the equivalent protons in a genuine solution non-equivalent in a damped liquid or environment. Thus, the changes of spectral features in Fig. 1B suggest the restricted movement of the groups, which is associated with the interaction between the polymer chains and MWCNTs. Certainly, only partial polymer chains are closely adhering to the surface of MWCNTs; thus, spectral features shown in Fig. 1A and 1B are largely similar.

The ^{13}C NMR spectra of **P1** and **1** are shown in Fig. S3.† The resonances of acetylene carbon atoms of **1** are observed at δ 82.6 and 80.5, which completely disappear in the spectrum of **P1**. Instead, two new peaks appear at δ 146.1 and 128.6, which can be assigned to the carbon atoms in the polyene backbone. This data again confirms that the triple bond of the monomer has been consumed by the polymerization reaction. Similar to the ^{1}H NMR spectrum, the resonances of the carbon atoms in the phenyl group directly attaching to the triple bond has a down-field shift from δ 114.7 to δ 125.3, due to the conjugation linking with polyene backbone after polymerization.

Raman shifts are sensitive to structural changes of MWCNTs. We detected the Raman shifts of the pristine MWCNTs and the hybrid of **P1**/MWCNTs, and the results are shown in Fig. 2. In the high frequency region from 1000 to 2000 cm^{-1}, the scattering peaks of MWCNTs appear at 1331 and 1578 cm^{-1}, which are assigned to the D- and G-bands, or the disordered and graphite-like bands of MWCNTs, respectively.[32–34] After hybridization with **P1**, the D- and G-bands shift to 1333 and 1585 cm^{-1}, respectively. It is obvious that the shift of the G-band (7 cm^{-1}) is more significant than that of D-band (2 cm^{-1}). The blue-shifting of G-band is normally associated with the isolation of carbon nanotubes (CNTs), which is referred as CNT diluting effect, indicating the decreasing of the π–π interaction between different CNTs. In the present case, the diluting effect is caused by the polymer chain wrapping on the surface of MWCNTs, which inserts an isolation layer between different MWCNTs. Moreover, according to the data in Fig. 2, the intensity ratios of the D- and G-bands are 0.38 and 0.36 before and after hybridization. The decrease of the D/G ratio indicates that the polymer wrapping is also a purification process for MWCNTs, and some disordered component has been removed due to its weaker interaction with the polymer chains.

It is well-known that D-mannose is a chiral molecule, thereby **P1** may demonstrate helical behavior in proper solvents. This was reported in our previous work and the tuning of the helicity by changing temperature and solvent was also

described.[14] It is a meaningful inference that the hybridization of the helical polymer with MWCNTs would impact on the helical property. Thus, we measured the temperature-dependent chirality variations of **P1** and the **P1**/MWCNTs hybrid in DMF solution. The circular dichroism (CD) spectrum of **P1** shows a peak at around 387 nm (Fig. S4†), indicating that the chiral pendant of D-mannose has successfully induced backbone helicity through chirality transfer from the pendant to the backbone. With elevating the temperature from 0 to 80 °C, the absolute [θ] value monotonously decreases, indicating the decrease of the helicity of the polymer backbone. This is in good agreement with the results reported in previous studies on helical poly(acetylenes).[6,35–39] It has been confirmed that Rh-complex catalyzed mono-substituted poly(acetylenes) usually have highly stereoregular head-to-tail *cis*-transoidal conformations, which are believed to be advantageous for helix induction.[35–39] Thus, the thermally induced *cis–trans* transition is a disadvantageous factor for preserving the chain helicity and the decrease of CD signal is expected to be observed.

The temperature-dependent variation of the helicity of **P1**/MWCNTs hybrid is shown in Fig. 4. In the whole temperature region, the CD signal for the hybrid is lower than the pure polymer. To quantitatively demonstrate the differences, the intensity of the CD signal, corresponding to the first Cotton effect (384 nm), is plotted *versus* the temperature. At the same temperature (20 °C) and polymer concentration (0.1 mM), the CD signal for **P1** is 13, about 1.3 times higher than that of **P2**/MWCNTs hybrid. The difference becomes smaller when the temperature is increased. At 80 °C, the CD intensity of the pure polymer and the hybrid are nearly equal. We propose a tentative explanation as follows. The polymer chains in the hybrids can be divided into three parts. The first part is the restricted polymer chains adhering to MWCNT's surface *via* π–π interaction, the second is the free polymer chains behaving identically to the pure polymer in DMF solution, and the third is the intermediate linking the above-mentioned two parts. Due to the π–π interaction, the phenyl groups are largely facing the surface of MWCNTs and the polymer main chains lose their helicity thus the first part has little contribution to the apparent [θ] value. The recorded CD signals originate from the second and the third parts. As a result, the absolute CD intensity for the hybrid is lower than that for pure **P1**. At high temperatures (*e.g.* 80 °C), the thermally induced stereo-isomerization of the D-mannose side groups greatly reduces the content of the one-handed helical sense of the polymer chains; thus, the pure polymer and the hybrid show similar CD intensity. When cooling the solution from 80 °C to 20 °C, the CD intensity recovers gradually but incompletely. For example, at 20 °C, the [θ] value is only 9.6, or 73.8% of its original intensity. The change of CD signal through thermally induced stereo-isomerization is reversible; therefore, the decrease in [θ] value must result from other factors, particularly the thermally induced *cis–trans* isomerization process, which is disadvantageous to the formation of helicity and the isomerization is irreversible at lowered temperatures. In contrast, at 20 °C, the [θ] value for the hybrid is about 9.0, or 90.9% of its original intensity (9.9), indicating better reversibility of the chain helicity. The π–π interaction between the polymer chains restrains the *cis–trans* isomerization and allows the hybrid to achieve a higher thermal stability.

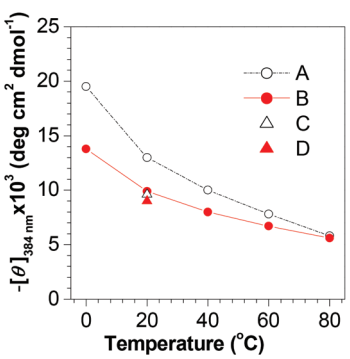

Fig. 4 The first Cotton effect at different temperatures. **P1** (A, C), **P1**/MWCNT (B, D). Heating process from 20 to 80 °C (A, B) and cooling process from 80 to 20 °C (C, D).

Another possible reason for the temperature-dependent CD intensity changes may be the thermally induced polymer degradation, which can lead to substantial and irreversible changes in chain helicity. In general, this is coincident with the data in Fig. 3 and 4. To verify the thermal effect, we examined the thermal stability of **P1** and the **P1**/MWCNTs hybrid with thermogravimetric analysis (TGA) technique and the data are displayed in Fig. S5.† **P1** begins to lose its weight at about 200 °C and loses 5% of its original weight at 223 °C (T_5), where T_5 is defined as the decomposition temperature. For the hybrid, T_5 increases to 293 °C. These data suggest that the degradation has not occurred to **P1** at 80 °C. Therefore, the temperature-dependent variation of the CD intensity cannot be attributed to thermally induced degradation.

Transmission electron microscopy (TEM) is a powerful technique to characterize the structure of the nanohybrids, and we used it to confirm the hybridization of **P1** and MWCNTs. As shown in Fig. 5A, the polymer itself tends to form spherical particles when precipitated from methanol. The particle size ranges from about 50 to 300 nm. The formation of sphere-shaped particles is determined by the fact that the protected mannose groups still have good hydrophilicity and high polarity, while the PPA backbones have high hydrophobicity and low polarity; thus, in highly polar precipitant methanol the polymer chains collapse into micelle-like particles.

In contrast, the precipitate obtained from the *in situ* polymerization resultant mixture showed remarkably different morphology. As revealed by the TEM image in Fig. 5B, a halo-like layer was surrounding a single MWCNT, indicating the coating of polymer chains onto the MWCNTs' surface. There could be two possible reasons for the polymer chain wrapping onto MWCNTs. (1) The monomers remain close to the MWCNT's surface through π–π interactions between the phenyl group of the monomer and the MWCNT's surface, and then polymerization is initiated and the polymer chains wrap on the surface.

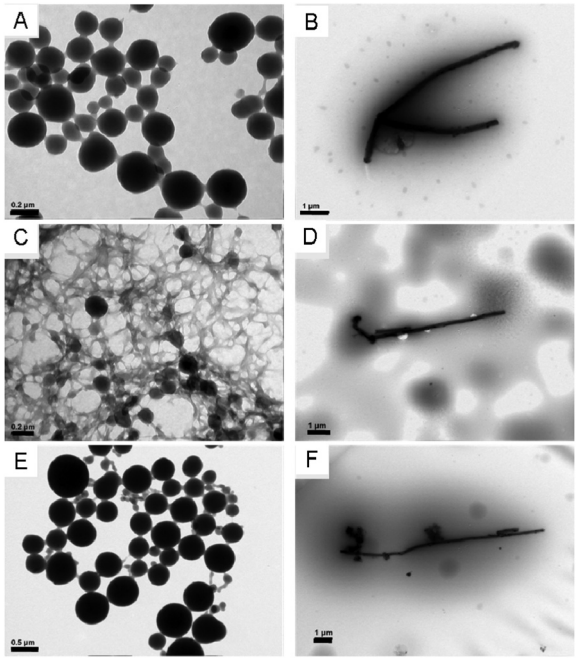

Fig. 5 TEM images of the polymers while being precipitated in methanol and the corresponding hybrids obtained by the precipitation of the *in situ* polymerization resultants in methanol. (A) P**1**, (B) P**1**/MWCNTs, (C) P**2**, (D) P**2**/MWCNTs, (E) P**3**, (F) P**3**/MWCNTs. Scale bar: (A, B) 200 nm, C 500 nm, (D, E, F) 1 μm.

(2) Part of the catalyst forms complexes with MWCNTs because Rh is highly affinitive to unsaturated hydrocarbons. Consequently, the polymerization occurs on the surface and the MWCNTs are spontaneously wrapped or coated by the polymer chains. The detailed mechanism is under investigation.

Fabrication and property of CS rods containing hybrids of monosaccharide-functionalized PPAs/MWCNTs

An important goal of the synthesis of monosaccharide functionalized PPAs and the preparation of the hybrids is to improve the biological friendliness and biocompatibility of the coating polymer layer on MWCNTs and to make use of the extraordinary tensile strength and structural flexibility of MWCNTs to reinforce the strength of CS rods. To this end, we fabricated CS rods containing the hybrids of monosaccharide-functionalized PPAs and MWCNTs through an *in situ* precipitation strategy, which had been reported in our previous works.[21,22] The fabrication of the CS rods containing P**1**/MWCNTs hybrid is briefly described here as an example. In acidic condition, P**1** undergoes a hydrolysis reaction and the protecting agent (acetone) is readily removed during the precipitation process (Scheme 2).[14,41] The hydrolysis recovers the protected mannose to its original form. The hydrolysis only results in an insignificant loss of the MWCNTs, because the sugar moieties populate mainly on the surface-layer of the hybrid, while the MWCNTs are surrounded by the hydrophobic polymer backbone *via* a π–π interaction.

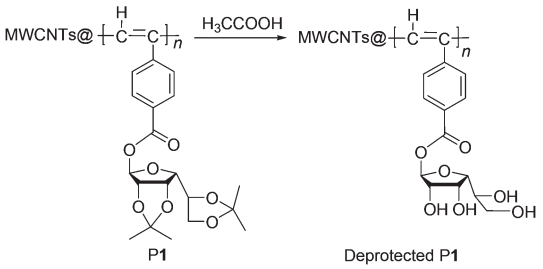

Scheme 2 Deprotection of the acetone protected D-mannose pendent of P**1** in P**1**/MWCNTs hybrid.

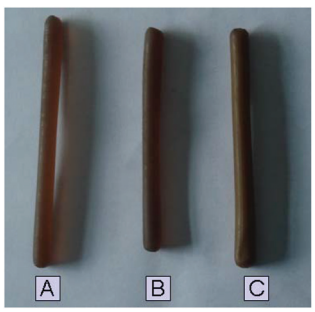

Fig. 6 Photographs of CS rods reinforced with: (A) hydrolyzed P**1**@MWCNTs; (B) hydrolyzed P**2**@MWCNTs; (C) hydrolyzed P**3**@MWCNTs.

Table 3 Bending strength and bending modulus of different CS rods[a]

Reinforced agent	Bending strength (MPa)	Bending modulus (GPa)
Blank (pure CS rods)	92.4[b]	4.1[b]
Hydroxyapatite (5%[c])	86.0[d]	3.4[d]
Hybrid of P**1**/MWCNTs (2.10%)	109.5	5.8
Hybrid of P**1** (2.10%)	94.5	4.6
Hybrid of P**2**/MWCNTs (2.35%)	118.9	5.7
Hybrid of P**3**/MWCNTs (2.79%)	120.6	6.0
Dikfix[e]	130.0	2.0–3.0

[a] The samples were determined by using the standard method of ANSI/ASAE S459-1993. [b] The data are extracted from ref. 21. In the present work, we measured the bending strength and modulus of pure CS rods in the same method as used for the evaluation of reinforced CS rods. [c] Weight percentage. [d] The data are extracted from ref. 16. [e] The data are extracted from ref. 16.

A representative photograph of the produced CS rods is shown in Fig. 6. The size of the cylindrical CS rod is in a length of 10 cm and a diameter of 5 mm. Based on the fabrication procedures, over 2.0% MWCNTs (by weight) were introduced into the CS rod. The bending strength and bending modulus of the fabricated CS rods were measured by using the standard method of ANSI/ASAE S459-1993. The data were collected by using the average values of five individual experiments and the results are summarized in Table 3. Moreover, the reference data of commercially available sample used in internal fixation of bone fractures (Dikfix Ltd, Co.), the pure

CS rods, composite CS rods reinforced with hydroxyapatite and **P1** are listed in Table 3.[16,22]

For instance, the bending strength and bending modulus of the CS rods reinforced with **P1**/MWCNTs hybrid are 109.5 MPa and 5.8 GPa, respectively. Quantitatively, these two key parameters are improved by 36.8% and 46.2% in comparison with the pure CS rods. The improvements in bending strength and bending modulus are 27.3% and 67.6% if compared with the CS rod reinforced with hydroxyapatite. In comparison with the CS rods reinforced with **P1**, these key parameters are 94.5 MPa and 4.6 GPa, indicating a certain enhancement. The enhancement effect can be associated with the rigidity of the conjugated polyphenylacetylene chain. When compared to commercial product (Dikfix) for the internal fixation of bone fracture, a fine result is that the bending modulus of the obtained CS rods is higher than Dikfix, while the bending strength is lower than Dikfix by about 15.8%. The CS rods reinforced by **P3**/MWCNTs present the best properties. The bending strength and bending modulus are 120.6 MPa and 6.0 GPa, respectively, which are evidently higher than that of pure CS rod and the CS rod reinforced with hydroxyapatite. In comparison with Dikfix, these two key parameters are higher and lower by 100% and 7.7%, respectively.

The improved performance of the CS rods reinforced by **P3**/MWCNTs over **P1**/MWCNTs can be partially ascribed to the higher loading of MWCNTs in the polymer matrix (Table 2). Thus, increasing the content of MWCNTs in the hybrids is a crucial factor to improve the bending strength of the hybrid CS rods, which can be expected that to be enhanced to the same level as Dikfix if the MWCNTs content can be higher, although substantial enhancement has been achieved by using the hybrids of the derived monosaccharide-functionalized PPAs and MWCNTs as reinforcement agents. We tried to carried out *in situ* polymerization in the presence of excess amount of MWCNTs, but the content of MWCNTs in the derived hybrids was only over 2% and no more than 3% (by weight, Table 2). It seems that the MWCNTs content in the polymer matrix is easy to increase by attaching fused and/or electron-donating aromatic moieties, such as pyrene, carbazole, and triphenylamine, to the side chains of PPA derivatives, as our previous works have shown; however,[2,26–30] their side effects on cells and tissues must be properly estimated. It is a propitious alternative to use MWCNTs of higher quality. As revealed by the morphology in Fig. 5, the MWCNTs used in this work have smaller specific ratio and length of the tubes has a wide distribution. It is rational that MWCNTs with larger specific ratio, uniform morphology and higher toughness would be good candidates as reinforcement agents.

In summary, we have synthesized three monosaccharide functionalized PPAs (**P1**–**P3**) with high molecular weight in high yield, and their structures have been well characterized. By using an *in situ* polymerization route, MWCNTs can be dispersed into polymer solutions and the loading factor of MWCNTs in polymer matrix is estimated in the range of 2%–3% by weight. As a result, hybrids of **P1**–**P3**/MWCNTs have been readily obtained. The interaction between the polymer main chain and MWCNTs were investigated with spectroscopic techniques (NMR and Raman), morphological observation (TEM) and thermogravimetric analysis (TGA). Following the *in situ* precipitation method, we successfully fabricated CS rods containing **P1**–**P3**/MWCNTs hybrids. The bending strength and bending modulus of the hybrid CS rods are substantially improved in comparison with the CS rods made from pristine CS and reinforced by hydroxyapatite. The bending strength of the obtained hybrid CS rods is lower than the commercially available product Dikfix. Accordingly, we are exploring better biocompatible units to modify the PPA structure and trying to introduce more high quality MWCNTs into the CS matrix and further improve the mechanical properties and friendliness of the hybrid CS rods.

Experimental section

Materials

Tetrahydrofuran (THF) was distilled under normal pressure from sodium benzophenone ketyl under nitrogen immediately prior to use. Triethylamine (Et_3N) was distilled and dried over potassium hydroxide. Dichloromethane (DCM) and acetone were distilled and dried over calcium hydride (CaH_2). 4-Ethynylbenzonic acid, *p*-toluene sulfonic acid monohydrate (TsOH), *N*,*N*′-dicyclohexyl-carbodiimide (DCC) and 4-(dimethylamino)pyridine (DMAP) were purchased from Acros. CuI, PPh_3, $(PPh_3)_2PdCl_2$, KOH, $AgNO_3$ were purchased from Aldrich. Organorhodium complexes $[Rh(nbd)Cl]_2$ (nbd = 2,5-norbornadiene) and $[Rh(cod)Cl]_2$ (cod = 1,8-cyclooctadiene) were prepared in our laboratory according to a literature method.[40] *N*,*N*-Dimethylformamide (DMF), chloroform, methanol and petroleum (b.p. 60–90 °C) solvents were of analytical grade and directly used as-received without further purification. The monosaccharides, *i.e.* D-mannose, D-glucose and D-galactose, were purchased from Aladdin.

Instruments

^1H and ^{13}C NMR spectra were measured on a Bruker ARX 500 NMR spectrometer using tetramethylsilane (TMS; δ = 0 ppm) as an internal standard. FTIR spectra were obtained on a Perkin Elmer 16 PC FT-IR spectrophotometer. Raman shifts were monitored on a RENISHAW inVia Raman Microscope. Molecular weights (M_w and M_n) and polydispersity indexes (PDI, M_w/M_n) of the polymers were estimated in THF by a Waters gel permeation chromatography (GPC) system. A set of monodisperse polystyrene standards covering molecular weight range of 10^3–10^7 were used for molecular weight calibration. UV-visible absorption spectra were measured on a Varian CARY 100 Bio UV-vis spectrophotometer. Circular dichroism (CD) spectra were recorded on an MOS-450 spectropolarimeter. The thermogravimetric analysis (TGA) was conducted on a Pyris 6 thermogravimetric analyzer (Perkin Elmer). The morphology of the samples were measured on a JEOL/JEM-200 CX transmission electron microscope (TEM) apparatus

working under an accelerating voltage of 160 kV, which was mounted with a EX500W CCD camera (GATAN). The SEM photographs were obtained using a JSM-5510 microscope.

Synthesis of monomers and polymers

The syntheses of the monomers (**1**, **2** and **3**) were reported elsewhere.[14] In the ESI,† we have provided detailed descriptions for the readers. For the polymerization, we described the preparation of P**1** as an example of the typical experimental procedures. All the polymerization reactions were performed under nitrogen using Schlenk technique in a vacuum-line system, except for the purification of the polymers, which was carried out in air.

In a 10 mL baked Schlenk tube with a side arm, 97 mg (0.25 mmol) of monomer **1** was added. The tube was evacuated under vacuum and flushed with dry nitrogen three times through the side arm. Then, 1.0 mL of THF was injected into the tube to dissolve the monomer. The catalyst solution was prepared in another tube by dissolving 5.8 mg (0.0125 mmol) of $[Rh(nbd)Cl]_2$ in 1 mL of THF with one drop of TEA added. After aging for 15 min, the catalyst solution was transferred to the monomer solution using a hypodermic syringe. The reaction system turned to black-brown from light yellow immediately. After being stirred at room temperature under nitrogen protection for 24 h, the resultant solution was diluted with 5 mL of THF and added dropwise to 300 mL of methanol through a cotton filter with vigorous stirring. The precipitate that was obtained was allowed to stand for 24 h, and then filtered with a Gooch crucible. The obtained polymer was washed with methanol for three times, and then maintained in an ambient atmosphere at room temperature. Note that dark red platelets were obtained, and the yield and molecular weight of the obtained polymer are given in Table 1. The characterization data of IR and NMR are demonstrated below.

Poly(2,3:5,6-di-*O*-isopropylidene-1-*O*-(4-ethynylbenzonyl)-α-D-mannofuranose) (P1). Red platelet solid. Characterization data: IR (KBr), ν (cm^{-1}): 1729 (s, C═O). ^1H NMR (300 MHz, $CDCl_3$), δ (TMS, ppm): 7.6 (aromatic protons *o*-C═O), 6.7 (aromatic protons *m*-C═O), 6.3 (CO_2CH), 5.7 (*cis*-olefin proton), 4.9 (C*H* in 4-mannofuranose), 4.8 (C*H* in 2-mannofuranose), 4.4 (m, 1H, CH_2 in 5-mannofuranose), 4.0 (C*H* in 3-mannofuranose, CH_2 in 6-mannofuranose), 1.6, 1.5, 1.4, 1.3 ($(CH_3)_2CO_2)_2$). ^{13}C NMR (75 MHz, $CDCl_3$), δ (TMS, ppm): 163.9 (CO_2), 146.1 (═*C*–), 139.2 (aromatic carbons *p*-C═O), 132.0 (aromatic carbon attached to C═O), 129.5 (aromatic carbons *o*-C═O), 128.4 (H*C*═), 127.0 (aromatic carbons *m*-C═O), 113.1, 109.0 ($(CH_3)_2CO_2)_2$), 101.5 (CO_2CH), 85.0, 82.5, 79.2, 72.9, 66.6 (*C*H in mannofuranose), 26.9, 26.0, 25.2, 24.6 ($(CH_3)_4$).

Poly(1,2:5,6-Di-*O*-isopropylidene-3-*O*-(4-ethynylbenzonyl)-α-D-glucofuranose) (P2). IR (KBr), ν (cm^{-1}): 1720 (s, C═O). ^1H NMR (300 MHz, $CDCl_3$), δ (TMS, ppm): 7.6 (aromatic protons *o*-C═O), 6.7 (aromatic protons *m*-C═O), 5.9 (C*H* in 1-glucofuranose), 5.6 (*cis*-olefin proton), 5.4 (CO_2CH), 4.5 (C*H* in 2-glucofuranose), 4.3 (C*H* in 4,5-glucofuranose), 4.0 (CH_2 in 6-glucofuranose), 1.5, 1.4, 1.2 ($(CH_3)_2CO_2)_2$). ^{13}C NMR (75 MHz, $CDCl_3$), δ (TMS, ppm): 164.2 (CO_2), 146.3 (═*C*–), 139.3 (aromatic carbons *p*-C═O), 132.1 (aromatic carbon attached to C═O), 129.3 (aromatic carbons *o*-C═O), 128.5 (H*C*═), 126.9 (aromatic carbons *m*-C═O), 112.3, 109.3 ($(CH_3)_2CO_2)_2$), 105.0 (*C*H in 1-glucofuranose), 83.3, 79.7, 76.8, 72.4, 67.0 (*C*H in glucofuranose), 26.7 ($(CH_3)_2$), 26.1, 25.3 ($(CH_3)_2$).

Poly(1,2:3,4-Di-*O*-isopropylidene-6-*O*-(4-ethynylbenzonyl)-D-galactopyranose) (P3). Yellow platelet solid. Characterization data: IR (KBr), ν (cm^{-1}): 1721 (s, C═O). ^1H NMR (300 MHz, $CDCl_3$), δ (TMS, ppm): 7.6 (aromatic protons *o*-C═O), 6.7 (aromatic protons *m*-C═O), 5.7 (*cis*-olefin proton), 5.5 (C*H* in 1-galactopyranose), 4.6 (C*H* in 3-galactopyranose), 4.3 (CO_2CH_2, C*H* in 2,4-galactopyranose), 4.1 (C*H* in 5-galactopyranose), 1.44, 1.33, 1.27 ($(CH_3)_2CO_2)_2$). ^{13}C NMR (75 MHz, $CDCl_3$), δ (TMS, ppm): 165.5 (CO_2), 146.1 (═*C*–), 139.7 (aromatic carbons *p*-C═O), 132.1 (aromatic carbon attached to C═O), 129.3 (aromatic carbons *o*-C═O), 128.8 (H*C*═), 127.0 (aromatic carbons *m*-C═O), 109.5, 108.6 ($(CH_3)_2CO_2)_2$), 96.1 (*C*H in 1-galactopyranose), 71.1 (*C*H in 2-galactopyranose), 70.0 (*C*H in 4-galactopyranose), 70.5 (*C*H in 3-galactopyranose), 66.1 (CO_2CH_2), 63.9 (*C*H in 5-galactopyranose), 25.9 ($(CH_3)_2$), 24.9, 24.5 ($(CH_3)_2$).

Preparation of hybrids of polymer/MWCNTs. Two schemes were used to prepare the hybrids of monosaccharide-functionalized poly(phenylacetylenes) and MWCNTs. (i) Dispersing MWCNTs into polymer solution by simple blending. Here, the preparation of P**1**/MWCNTs hybrid is described as an example. 10 mg P**1** was dissolved in 5 mL $CHCl_3$, and 10 mg MWCNTs were added into the solution. After ultrasonication for 15 min, the mixture was filtered through a cotton filter to remove insoluble MWCNTs. The filter was dried before and after filtration in an oven at 100 °C under vacuum to constant weight. The concentration of SWNT in $CHCl_3$ was calculated by a reported method. (ii) Hybridization of MWCNTs with polymers by *in situ* polymerization. The polymerization reaction of monosaccharide-functionalized PPA was carried out in the presence of a proper amount of MWCNTs. After polymerization, the resultant mixture was diluted with THF, and the solution/suspension was filtered through a cotton filter to remove insoluble MWCNTs.

Fabrication of CS rods reinforced with hybrids of polymer/MWCNTs. Based on our reported *in situ* precipitation art,[10,11] experimental details of a typical run are described as following. 180 mL acetic acid aqueous solution (2%, by volume) was added into a 220 mL aqueous solution containing polymer/MWCNTs hybrids. 20 g CS was added into the above mixture under with stirring for 1 h. A sol of CS containing polymer/MWCNTs hybrids was generated. The sol was kept maintained still for 24 h to release the trapped air bubbles, and then injected into a cylindrical mold. Immersing the mold in sodium hydroxide aqueous solution (5%, wt) for 6 h, and the CS sol gradually turned into CS gel in a rod shape. The fabricated CS rods were washed with deionized water several times to remove the resultant salts and acetone formed in the de-protection of the sugar moieties and in the neutralization

treatment. Finally, the rods were air-dried in oven at 60 °C. The dried CS rods (diameter: 5 mm, length: 10 cm) were sent for the determination of bending strength and bending modulus.

Acknowledgements

This work was partially supported by the National Basic Research Program of China (973 program; 2013CB834704), the National Science Foundation of China (51273175), and the Research Grants Council of Hong Kong (604711, 602212 and HKUST2/CRF/10). J. Z. Sun acknowledges the support from Jiangsu Key Laboratory of Advanced Functional Polymer Design and Application (Soochow University).

Notes and references

1 W. F. Li, H. J. Huang, Y. Li and J. P. Deng, *Polym. Chem.*, 2014, **5**, 1107.
2 J. Z. Sun, A. Qin and B. Z. Tang, *Polym. Chem.*, 2013, **4**, 211.
3 M. Shiotsuki, F. Sanda and T. Masuda, *Polym. Chem.*, 2011, **2**, 1044.
4 K. Akagi, *Chem. Rev.*, 2009, **109**, 5354.
5 J. Z. Liu, J. W. Y. Lam and B. Z. Tang, *Chem. Rev.*, 2009, **109**, 5799.
6 E. Yashima, K. Maeda, H. Iida, Y. Furusho and K. Nagai, *Chem. Rev.*, 2009, **109**, 6102.
7 B. M. Rosen, C. J. Wilson, D. A. Wilson, M. Peterca, M. R. Imam and V. Percec, *Chem. Rev.*, 2009, **109**, 6275.
8 J. G. Rudick and V. Percec, *Acc. Chem. Res.*, 2008, **41**, 1641.
9 T. Masuda, *J. Polym. Sci., Part A: Polym. Chem.*, 2007, **45**, 165.
10 J. W. Y. Lam and B. Z. Tang, *Acc. Chem. Res.*, 2005, **38**, 745.
11 B. Li, K. K. L. Cheuk, F. Salhi, J. W. Y. Lam, J. A. K. Cha, X. Xiao, C. Bai and B. Z. Tang, *Nano Lett.*, 2001, **1**, 323.
12 B. Z. Tang, *Polym. News*, 2001, **26**, 262.
13 K. K. L. Cheuk, B. S. Li, J. W. Y. Lam, Y. Xie and B. Z. Tang, *J. Polym. Sci., Part A: Polym. Chem.*, 2008, **41**, 5997.
14 K. K. L. Cheuk, J. W. Y. Lam, B. S. Li, Y. Xie and B. Z. Tang, *Macromolecules*, 2007, **40**, 2633.
15 J. W. Y. Lam, K. K. L. Cheuk, B. S. Li, Y. Xie and B. Z. Tang, *Chin. J. Polym. Sci.*, 2007, **25**, 119.
16 Z. K. Wang, H. Zhao, L. Fan, J. Lin, P. Zhuang, W. Z. Yuan, Q. L. Hu, J. Z. Sun and B. Z. Tang, *Carbohydr. Polym.*, 2011, **84**, 1126.
17 A. Di Martino, M. Sittinger and M. V. Risbud, *Biomaterials*, 2005, **26**, 5983.
18 K. C. Gupta and F. H. Jabrail, *Int. J. Biol. Macromol.*, 2006, **38**, 272.
19 L. Moroni and J. H. Elisseeff, *Mater. Today*, 2008, **11**, 44.
20 A. E. Nel, L. Madler, D. Velegol, T. Xia, E. M. V. Hoek and P. Somasundaran, *Nat. Mater.*, 2009, **8**, 543.
21 Q. L. Hu, X. Z. Qian, B. Q. Li and J. C. Shen, *Chem. J. Chin. Univ.*, 2003, **24**, 528.
22 Q. L. Hu, B. Q. Li, M. Wang and J. C. Shen, *Biomaterials*, 2004, **25**, 779.
23 Q. L. Hu, F. P. Chen, B. Q. Li and J. C. Shen, *Mater. Lett.*, 2006, **60**, 368.
24 Z. K. Wang, Q. L. Hu, X. G. Dai, H. Wu, Y. X. Wang and J. C. Shen, *Polym. Compos.*, 2009, **30**, 1517.
25 J.-H. Ke, Z.-K. Wang, Y.-Z. Li, Q.-L. Hu and J. Feng, *Chin. J. Polym. Sci.*, 2012, **30**, 436.
26 W. Z. Yuan, J. Z. Sun, Y. Q. Dong, M. Häußler, F. Yang, H. P. Xu, A. Qin, J. W. Y. Lam, Q. Zheng and B. Z. Tang, *Macromolecules*, 2006, **39**, 8011.
27 W. Z. Yuan, Y. Mao, H. Zhao, J. Z. Sun, H. P. Xu, J. K. Jin, Q. Zheng and B. Z. Tang, *Macromolecules*, 2008, **41**, 701.
28 H. Zhao, W. Z. Yuan, L. Tang, J. Z. Sun, H. P. Xu, A. Qin, Y. Mao, J. K. Jin and B. Z. Tang, *Macromolecules*, 2008, **41**, 8566.
29 H. Zhao, W. Z. Yuan, J. Mei, L. Tang, X. Q. Liu, J. M. Yan, X. Y. Shen, J. Z. Sun, A. Qin and B. Z. Tang, *J. Polym. Sci., Part A: Polym. Chem.*, 2009, **47**, 4995.
30 W. Z. Yuan, A. Qin, J. W. Y. Lam, J. Z. Sun, M. Haussler, J. Liu, H. P. Xu, Q. Zheng and B. Z. Tang, *Macromolecules*, 2007, **40**, 3159.
31 J. Z. Sun, H. Z. Chen, R. S. Xu, M. Wang, J. W. Y. Lam and B. Z. Tang, *Chem. Commun.*, 2002, 1222.
32 A. M. Rao, E. Richter, S. Bandow, B. Chase, P. C. Eklund, K. A. Williams, S. Fang, K. R. Subbaswamy, M. Menon, A. Thess, R. E. Smalley, G. Dresselhaus and M. Dresselhaus, *Science*, 1997, **275**, 187.
33 A. C. Ferrari, J. C. Meyer, V. Scardaci, C. Casiraghi, M. Lazzeri, F. Mauri, S. Piscanec, D. Jiang, K. S. Novoselov, S. Roth and A. K. Geim, *Phys. Rev. Lett.*, 2006, **97**, 187401.
34 K. N. Kudin, B. Ozbas, H. C. Schniepp, R. K. Prud'homme, I. A. Aksay and R. Car, *Nano Lett.*, 2008, **8**, 36.
35 J. S. Moore, C. B. Gorman and R. H. Grubbs, *J. Am. Chem. Soc.*, 1991, **113**, 1704.
36 Y. Kishimoto, M. Itou, T. Miyatake, T. Ikariya and R. Noyori, *Macromolecules*, 1995, **28**, 6662.
37 B. Z. Tang, X. Kong, X. Wan and X.-D. Feng, *Macromolecules*, 1997, **30**, 5620.
38 E. Yashima, Y. Maeda and Y. Okamoto, *Nature*, 1999, **399**, 449.
39 T. Aoki, T. Kaneko, N. Maruyama, A. Sumi, M. Takahashi, T. Sato and M. Teraguchi, *J. Am. Chem. Soc.*, 2003, **125**, 6346.
40 R. R. Schrock and J. A. Osborn, *Inorg. Chem.*, 1970, **9**, 2339.
41 K. Yasugi, T. Nakamura, Y. Nagasaki, M. Kato and K. Kataoka, *Macromolecules*, 1999, **32**, 8024.

